High-efficiency broadband blazed metagrating working in visible light

IOP Publishing Journal of Optics
J. Opt. **25** (2023) 025002 (7pp) https://doi.org/10.1088/2040-8986/acac40

High-efficiency broadband blazed metagrating working in visible light

Yu Lin, Yeming Han, Chengmiao Wang, Bowen Li, Jianyu Zhang and Yongbo Deng*

State Key Laboratory of Applied Optics (SKLAO), Changchun Institute of Optics, Fine Mechanics and Physics (CIOMP), Chinese Academy of Sciences, Dongnanhu Road 3888, Changchun 130033, People's Republic of China

E-mail: dengyb@ciomp.ac.cn

Received 15 September 2022, revised 8 December 2022
Accepted for publication 16 December 2022
Published 29 December 2022

Abstract

A simple 1D blazed metagrating is proposed. The metagrating consists of SiO_2 film sandwiched by Ag substrate and Ag nanostrips, which can achieve high-efficiency −1st-order diffraction in the range of 550 nm to 700 nm, and the peak efficiency is nearly 98%. The SiO_2 dielectric layer in previous designs is used chiefly as a waveguide layer to support a guided mode. In comparison, it is introduced here to suppress the unwanted diffraction order (zero-order), which helps achieve high-efficiency diffraction at a high diffraction order. For analysis, the metagrating is disassembled into two parts, including a flat plate and a grating. By analysing the far-field radiation pattern of scattered waves and the reflection phase of a specific mode for these two parts, we conclude that the cause of high-efficiency blazing draws support from suppressing zero-order based on destructive interference. This work provides an intuitive physical image for this type of metagrating and an idea to design high-efficiency diffraction and beam deflection devices from the perspective of interference.

Keywords: metagrating, diffraction, blazed grating, destructive interference

(Some figures may appear in colour only in the online journal)

1. Introduction

Diffraction optics is an ancient and essential branch of optics. Diffraction devices play a vital role in beam manipulation, which are expected to deflect incident light into a specific direction (high diffraction order) with high efficiency. Diffraction grating is a critical diffraction device, and diffraction grating has a long history. '*No single tool has contributed more to the progress of modern physics than the diffraction grating* [1] …' The development of grating has promoted the development of optics. The fundamental idea of the grating can be applied in many current micro-nano structures that manipulate electromagnetic fields [2, 3]. What are the applications of diffraction in specific directions? The realization of efficient directional diffraction has many applications in the spectral analysis [4–6], holographic display [7–9], imaging [10, 11], mode selectivity and coupling [12, 13], and other fields. The conventional way to effectively direct energy to high diffraction orders is completed by a blazed grating with triangular grooves, working under the Littrow configuration [14]. The core of blazed gratings is to keep the zero-order radiation direction of the grating unit consistent with the specific diffraction order radiation direction of the entire grating; then, the radiation interference among units can accomplish the high-efficiency high-order diffraction. However, the conventional blazed gratings, exhibiting linear surface profiles, suffer from a strong shadowing effect that drastically reduces the diffraction efficiency of the element [15]. In the Littrow configuration, the incident and diffracted light are in the same direction, leading to difficulties in actual detection. For developing traditional grating, it is worth mentioning that some researchers

* Author to whom any correspondence should be addressed.

have proposed a single-layer rod grating [16], which can realize the high-efficiency energy conversion between zero-order and −1st-order in broadband and a wide angle range. This earlier work of nearly perfect blazed grating has essential reference significance for beam deflection and directional radiation. Recently, with the development of nano-processing technology, the appearance of metasurfaces [17, 18] provides a new way for beam manipulation. The gradient arrangement of some structures on the material surface can realize the beam deflection at any angle. Since the introduction of the metasurface, it has attracted much attention. There has been much work to use the metasurface to achieve beam deflection, directional radiation, and many other applications [19–21]. Nonetheless, metasurface is challenging to achieve high-efficiency directional radiation by structures with discretized phases [11, 22]. In addition, the structure is more complex than the conventional gratings and challenging to fabricate. In addition to the above two methods, Ra'di *et al* [22] proposed the concept of metagratings, which enables unitary efficiency without the need for deeply subwavelength elements, turning away from the discretization of a continuous phase or impedance profile. Metagratings are periodic or locally periodic arrays working in the few-diffraction order (FDO) regime [11, 23]. Different from metasurfaces, metagratings are set the periodically to align the direction of one of the propagating higher-order Floquet modes with the desired direction of reflection, which engineers scattered in each unit cell so that its radiation field has nulls in the direction of all propagating Floquet modes other than the one that is aligned with the desired direction of reflection [24].

Due to the high feasibility of metagrating in beam deflection and directional radiation, it has attracted much attention. Recently, the research on metagratings has covered microwave [22, 25, 26], millimeter-wave frequencies [27], terahertz [28–30], and visible optical regimes [9, 15, 31–33]. In optical regimes, Shi *et al* [31] proposed a kind of kissing-dimer metagrating that can universally achieve high diffraction efficiencies in the visible range. The metagrating they proposed possesses 90% diffraction efficiency; it is worth noting that their work can produce high diffraction efficiency over wide bandwidths from 450 nm to 1000 nm. Nevertheless, the peak diffraction efficiency is not very high, and the structure is relatively complex. Deng *et al* [9] designed a metagrating with a peak efficiency of 93%, and their structure is easy to fabricate. However, the peak efficiency is not high enough too. Oliva *et al* [15] proposed high-efficiency broadband blazed grating in the resonance domain. They show that the moderate maximum diffraction efficiency (70%) of a two-bar binary grating for a normal incident wave from air to the substrate can be significantly increased to 90% by a subsequent mode conversion layer. The above excellent works still have some disadvantages, such as complex structure or not with high peak efficiency. Some metagratings with high diffraction efficiency based on simple structures have been proposed [23, 34]. They are mainly based on the coupling between modes to extract the energy to a specific radiation channel, which mostly depends on the resonance effect. The quality factor of the structure is high, and it is not easy to achieve high-efficiency diffraction in broadband. All the above studies suggest that metagratings are considered as the potential devices for deflecting light beams in the future.

Here, we propose a simple 1D metal metagrating working in visible light, which can achieve high-efficiency −1st-order diffraction at a range of incident wavelengths and angles; the peak efficiency of the designed metagrating can reach nearly 98%. We decompose the metagrating into two parts, including a silicon dioxide (SiO_2) film covered on a silver (Ag) substrate and an Ag grating. For these two parts, the far field of the scattered waves and the reflection phase of the specific mode (zero-order reflection) obeying Snell's law [35] are calculated, respectively. After analysis, we found that the high-efficiency blazing originates from the effective interference inside the metagrating. The zero-order diffraction is perfectly suppressed by the destructive interference in the metagrating, thus realizing high-efficiency blazing. We try to explain high-efficiency blazing from the perspective of interference.

2. Simulation and results

We propose a metagrating, as shown in figure 1(a), and the structural unit parameters are shown in figure 1(b). Schematic view of a metagrating in figure 1, the same colour represents the same material.

We use the Fourier mode method (FMM) [36–39] for numerical calculation, and the refractive indexes of Ag and SiO_2 come from here [40]. We will briefly review the core idea and basic implementation process of the FMM. First, the dielectric constant with the periodic distribution in the metagrating region is expandable in a Fourier series of the form, which can be expressed as [39]

$$\varepsilon(x) = \sum_h \varepsilon_h \exp\left(\mathrm{j}\frac{2\pi h}{\Lambda}\right), \tag{1}$$

where h is the hth Fourier component of the relative permittivity in the grating region, j is an imaginary unit, and Λ is the grating period. '*The general approach for solving the exact electromagnetic-boundary-value problem associated with the grating is to find solutions that satisfy Maxwell's equations in each of the three (input, grating, and output) regions and then match the tangential electric- and magnetic-field components at the two boundaries* [39].' We will retell the grating region in more detail. As for the transverse magnetic (TM) polarized (the magnetic field vector parallel to the y-axis) plane wave with an incident angle $\theta_0 = 0°$ is used as the excitation source. The grating region ($0 < z < d_g$) the tangential magnetic (y-component) and electric (x-component) fields may be expressed as a Fourier expansion form:

$$H_{gy} = \sum_i U_{yi}(z)\exp(-\mathrm{j}k_{xi}x) \tag{2}$$

$$E_{gx} = -\mathrm{j}\left(\frac{\mu_0}{\varepsilon_0}\right)^{\frac{1}{2}} \sum_i S_{xi}(z)\exp(-\mathrm{j}k_{xi}x) \tag{3}$$

where $U_{yi}(z)$ and $S_{xi}(z)$ are the normalized amplitudes of the ith space-harmonic fields, μ_0 is the permeability of free space,

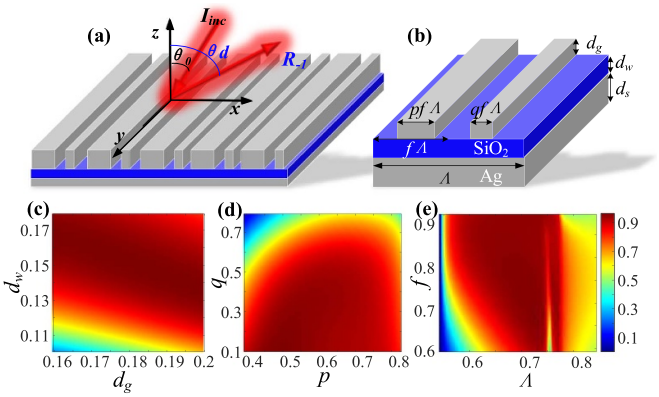

Figure 1. Schematic view of a metagrating geometry and dependence of diffraction efficiency on parameters. (a) Globe structure of a metagrating; (b) unit of the metagrating; (c)–(e) the dependence of −1st-order diffraction efficiency on structural parameters.

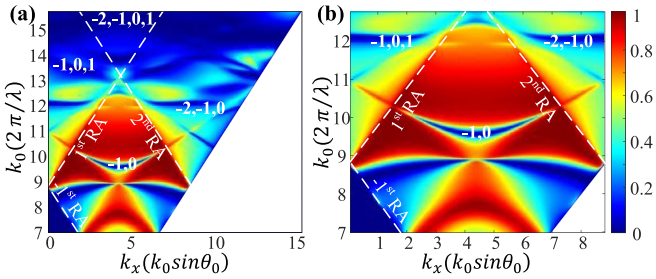

Figure 2. Diffraction efficiency and diffraction order chart. (a) The relationship between −1st-order diffraction efficiency and wave vectors; the white dotted line is the RAs for diffraction orders; (b) details of the region of interest of (a).

ε_0 is the permittivity of free space. k_{xi} is the parallel wave vector of the ith diffracted wave, which is determined from the Floquet condition [39] and is given by

$$k_{xi} = k_0\left[n\sin\left(\theta_0\right) - \mathrm{i}\left(\frac{\lambda}{\Lambda}\right)\right] \tag{4}$$

Where λ is the incident wavelength, $k_0 = 2\pi/\lambda$ the wave vector of free space. $U_{yi}(z)$ and $S_{xi}(z)$ satisfy Maxwell's equations so that we can get

$$\frac{\partial H_{gy}}{\partial z} = -\mathrm{j}\omega\varepsilon_0\varepsilon(x)E_{gx}, \tag{5}$$

$$\frac{\partial E_{gx}}{\partial z} = -\mathrm{j}\omega\mu_0 H_{gy} + \frac{\partial E_{gx}}{\partial x} \tag{6}$$

where the ω is the angular optical frequency. Substituting equations (2) and (3) into equations (5) and (6) and eliminating H_{gy}, we can get the set of coupled-wave equations

$$\begin{bmatrix} \partial\mathbf{U}_y/\partial(z') \\ \partial\mathbf{S}_x/\partial(z') \end{bmatrix} = \begin{bmatrix} 0 & \mathbf{E} \\ \mathbf{B} & 0 \end{bmatrix}\begin{bmatrix} \mathbf{U}_y \\ \mathbf{S}_x \end{bmatrix}, \tag{7}$$

where $\mathbf{B} = \mathbf{K_x}\mathbf{E}^{-1}\mathbf{K_x} - \mathbf{I}$, $\mathbf{E}$ is the matrix formed by the permittivity harmonic components, $\mathbf{K_x}$ is a diagonal matrix, with the i, i element being equal to k_{xi}/k_0, $z' = k_0 z$, and $\mathbf{I}$ is the identity matrix. Equation (7) is obtained so that we can match the boundary conditions of tangential electromagnetic field components above and below the grating region, solve Maxwell equations, and get the efficiency of different reflective diffraction orders of the grating as

$$\mathrm{DE_{ri}} = R_i R_i^* Re\left(\frac{k_{\mathrm{in,zi}}}{k_0 n_{\mathrm{in}}\cos(\theta_0)}\right), \tag{8}$$

R_i is the normalized electric-field amplitude of the ith backward-diffracted (reflected) wave in input. $k_{\mathrm{in,zi}}$ is the vertical wave vector component for ith backward-diffracted (reflected) wave of the input, n_{in} is the refractive index of one side of the input, θ_0 is the incident angle, and * and Re represents the complex conjugate and real parts, respectively. Please refer to the papers [37, 39] for specific parameter-solving methods and further understanding.

To obtain a better structure, we divide the structural parameters into three groups; p and q are one group, f and Λ are one group, and d_g and d_w are the other group; The structure with higher −1st-order diffraction efficiency was obtained by paired parameter scanning. Figures 1(c) and (d) show the relationship between the diffraction efficiency and the metagrating parameters. Through these three figures, we find the metagrating parameters for high-efficiency blazing. When the parameters are $\Lambda = 713$ nm, $f = 0.7$, $p = 0.49$, $q = 0.1$, $d_g = 187$ nm, and $d_w = 146$ nm, we calculate the −1st-order diffraction efficiency under different wave vectors. The numerical calculation model is equivalent to vertically flipping the metagrating in figure 1(b). The calculation uses a plane wave with TM polarization as the excitation source. The structure was simulated by employing periodic conditions along the x-axis and a perfectly matched layer along the z-axis. The coordinate system selected for calculation is shown in figure 1(a). The dependence of −1st-order diffraction efficiency on wave vectors is shown in figures 2(a) and (b) shows the details of the region of interest in (a). The white dotted line in figure 2 is the Rayleigh anomalies (RAs) [23, 41] for diffraction orders, which can be calculated by the grating equation

$$k_x \pm \tfrac{2i\pi}{\Lambda} = \pm k_0. \tag{9}$$

In the equation, where $k_0 = 2\pi/\lambda$ is the wave vector in a vacuum, k_x is the parallel wave vector, λ is the wavelength of the incident light, Λ is the period of the metagrating. The high-efficiency diffraction of the metagrating generally works in the FDO regime [11, 23]. To achieve high-efficiency blazing in an FDO regime, we selected the wave vector region with only zero-order and −1st-order diffraction, as shown in figure 2(b), for numerical analysis.

Next, we analyse the selected FDO region; we show the optical performance of the metagrating in figure 3. The reflection spectra show that the metagrating can achieve high efficiency blazing in a wide band. From 550 nm to 700 nm, the average reflection efficiency of the metagrating can reach 88%; and the average efficiency from 586 nm to 700 nm can reach 94%. When the wavelength is 591 nm, the peak

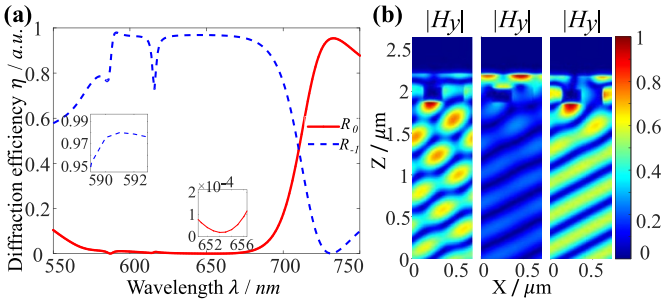

Figure 3. Optical performances of the metagrating. (a) The diffraction efficiency of zero-order (solid red line) and −1st-order (dotted blue line) varies with wavelengths. Electromagnetic field (|*Hy*|) distribution at incident wavelengths of 591 nm, 614 nm, and 654 nm.

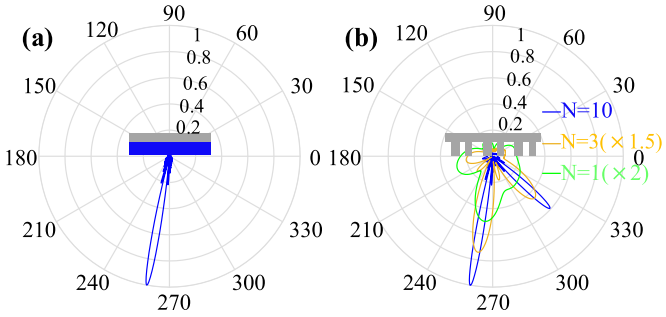

Figure 4. The far-field radiation pattern of the scattered wave. (a) The far-field radiation of the scattered waves for the SiO2 plate on the Ag substrate, the thickness of the SiO2 ($d_w = 146$ nm) is the same as above; (b) the far-field radiation of $N = 1$ (solid green line), 3 (solid orange line), and 10 (solid blue line), and the parameters of the Ag grating are consistent with the above.

efficiency can be close to 98%, which can be perceived from the blue dotted line in the inset of figure 3(a). At the wavelength of 654 nm, the zero-order diffraction is most obviously suppressed, as seen from the solid red line in the inset of figure 3(a). Why is the high peak efficiency here? We will describe it in detail later. To further analyse the optical performance of the metagrating, we calculated the distribution of the *y*-component of the magnetic field at different wavelengths. Figure 3(b) shows the normalized magnetic field intensity distribution at incident wavelengths of 591 nm, 641 nm, and 654 nm, respectively. The second column of near-field distribution in figure 3(b) shows that a large part of the energy is localized on the metal surface, causing absorption, which affects the diffraction efficiency of −1st-order; this is precisely consistent with the reflection concave of the reflection spectrum in figure 3(a). At 591 nm and 654 nm, a 'clean' near-field distribution with inconspicuous 'secondary scattering phenomena' can be perceived. Efficient reflection can be achieved, and zero-order diffraction must be well suppressed, illustrated by the 'clean' near-field distribution. The numerical results above lead us to think about how the zero-order is suppressed in this structure to achieve high-efficiency −1st-order diffraction.

3. Analysis and discussion

In order to answer our above questions, we calculated the normalized far-field radiation patterns of pure SiO_2 plate on Ag substrate and Ag grating by commercial software COMSOL Multiphysics [42], respectively. The calculation parameters are the same as those in the previous text. The results of the numerical simulation are shown in figure 4. Figure 4(a) shows that the zero-order radiation direction obeys Snell's law with high far-field power. In figure 4(b), we calculated the far-field radiation diagram, including $N = 1$, 3, and 10 periodic Ag grating, respectively (to observe the changing trend clearly, we enlarged the results of $N = 1, 3$). We can see that with the continuous increase of the number of periods, the energy gradually concentrates in two radiation directions; in other words, the energy is concentrated in the zero-order and the −1st-order. The above phenomenon is due to the interference among secondary scattering from multiple units. Finally, the energy is concentrated at the zero-order and −1st-order. From the far-field radiation pattern of scattered waves, we assume that the zero-order radiation of the SiO_2 plate and Ag grating are cancelled in the metagrating by destructive interference, which leads to the redistribution of energy in the metagrating and the realization of high-efficiency blazing.

To analyse and explain the above conjecture more quantitatively, we calculated the reflection phase of zero-order (normal reflection) obeying Snell's law for SiO_2 plate on Ag substrate and Ag grating. The problem studied in this work does not include the transmission field. The field at the reflection port can be expressed as [42]

$$\boldsymbol{E_{tot}} = \boldsymbol{E}_0 + \sum S_i \boldsymbol{E_i}, \tag{10}$$

where $\boldsymbol{E_{tot}}$ is the total field, $\boldsymbol{E}_0$ is the excitation field, $\boldsymbol{E_i}$ is the corresponding *i*th-order backward diffraction field, and S_i is the scattering coefficient of the *i*th diffraction order. The scattering coefficient can be calculated by

$$S_i = \frac{\int((\boldsymbol{E_{tot}} - \boldsymbol{E}_0).\boldsymbol{E}_0^*)dl}{\int(\boldsymbol{E_i}.\boldsymbol{E_i}^*)dl}, \tag{11}$$

where * represents the complex conjugate, and l represents the port length in the 2D calculation model. The phase is obtained by taking the argument of the scattering coefficient $\phi = \arg(S_i)$. The reflection phase at different wavelengths calculated by the above method is shown in figure 5. The solid red line represents the reflection phase of the SiO_2 plate on the Ag substrate ϕ_{SiO_2}, while the solid black line represents the zero-order reflection phase of the Ag grating ϕ_{Ag}. We make a difference between the two reflection phases and take the absolute value $|\Delta\phi| = |\phi_{SiO_2} - \phi_{Ag}|$, which is represented by a blue dotted line. For reference, we draw a green dotted line to indicate that the phase value is π. Interestingly, the phase differences $|\Delta\phi|$ of the waveband with high-efficiency blazing are around the π. What is more interesting is that the phase differences at 591 nm and 654 nm are almost π. Zero-order diffraction is perfectly suppressed at two wavelengths above,

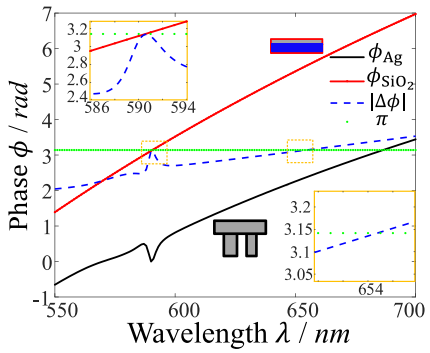

Figure 5. The dependence of reflection phase on wavelengths for SiO_2 plate on Ag substrate and Ag grating. The inset shows the local details of the phase differences approaching the π.

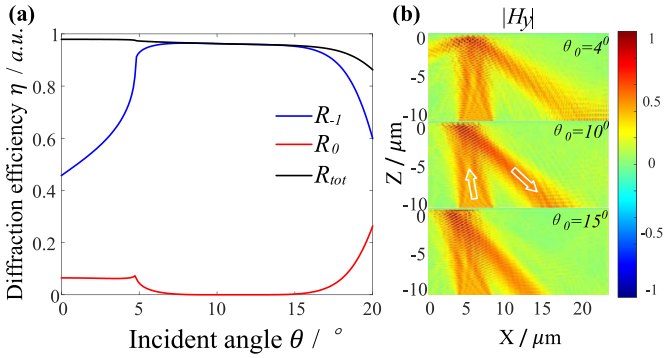

Figure 6. Diffraction performances vary with incident angles. (a) Diffraction efficiency varies with incident angles at a wavelength of 654 nm; (b) electromagnetic field distribution of incident light beam with finite width at a wavelength of 654 nm. The numerical simulation structure includes 40 periods, and the size of the calculation area is $38\lambda \times 18\lambda$. White arrows represent the direction of incoming and outgoing light.

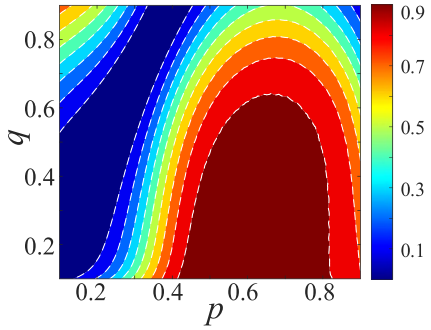

Figure 7. 1st-order diffraction efficiency at 654 nm for Ag nanostrips with different widths.

and high-efficiency −1st-order diffraction is achieved, which can be seen in combination with the insets of figures 3 and 5. The results support our assumption that destructive interference suppresses the zero-order, which leads to energy redistribution and high-efficiency blazing.

The use of diffractive devices generally has an angle tolerance. Next, we analyse the reflection efficiency of 654 nm (the red light commonly used in lasers or holographic display fields) at various incident angles. The parameters of the metagrating are consistent with the previous text. The results in figure 6(a) show that the metagrating can still achieve high-efficiency −1st-order reflection at a range of incident angles. The average reflection efficiency from 5 to 18° can reach 94%. To observe the blazing effect of the device more intuitively, we set the incident plane wave with finite width. The incident light beam width is seven times the period of the metagrating; the metagrating contains 40 periods. The calculated size is $38\lambda \times 18\lambda$. Figure 6(b) shows the y-component of the magnetic field when the incident angle is 4°, 10°, and 15°, respectively. The phenomenon of high-efficiency reflection can be perceived through the near-field distribution. When the incident angle is 4°, zero-order is not well suppressed, and the efficiency of −1st-order reflection efficiency is not as high as that of the incident angle of 10° and 15°. Obviously, metagrating can be used in a range of incident angles.

To prove our design is not a 'castle in the air,' we evaluated the manufacturability and manufacturing tolerance of the metagrating. For our proposed structure, as in figure 1, the waveguide layer and the refractive index modulation region (i.e. the region of Ag nanostrips), their thicknesses, and their heights are not challenging to process [43]. However, Ag nanostrips that are too thin and tall (large depth-to-width ratio) will lead to processing problems, so it is more important to control the width of the nanostrips, i.e. the parameters p and q in the structure. We calculated the diffraction efficiency under different p and q values (different line widths of Ag nanostrips). The results in figure 7 show that the linewidth has a manufacturing tolerance of tens of nanometres ($\Delta = \delta p\,(\delta q) f\Lambda$), which can ensure that the −1st-order diffraction efficiency at 654 nm is greater than 90% in an extensive range of Ag nanostrips widths. The result proves the possibility of the practical application of the metagrating, and we hope that the design will be applied in practice as soon as possible.

4. Summary

In summary, we propose a simple 1D metal metagrating. The metagrating is constructed on an Ag substrate, including SiO_2 film and Ag nanostrips. The average reflection efficiency of the metagrating can reach 94% in the bandwidth of nearly 120 nm, of which the peak efficiency is nearly 98%. The average reflection efficiency of the metagrating in the range of incident angle from 5° to 18° is as high as 94%, which is with incident angle tolerance. We decompose the metagrating into two parts: SiO_2 film on Ag substrate and Ag grating. We calculated the far-field radiation patterns of the scattered wave and the reflection phases of their specific modes (normal reflection) for these two structures. We try to explain that the high-efficiency −1st-order reflection is derived from the destructive interference cancellation of zero-order diffraction inside the metagrating through the above analysis. We provide a way of realizing high-efficiency blazing by suppressing the zero-order based on destructive interference. Further, this simple idea is conducive to using physical intuition to design the corresponding devices. The practical implementation is to accurately design

the waveguide layer's thickness to provide destructive interference to suppress unwanted diffraction orders. The work can be extended to other wavebands, which can provide a way to manipulate beam deflection.

Data availability statement

The data that support the findings of this study are available upon reasonable request from the authors.

Funding

Innovation Grant of Changchun Institute of Optics, Fine Mechanics and Physics (CIOMP); Fund of State Key Laboratory of Applied Optics (SKLAO); Youth Innovation Promotion Association of the Chinese Academy of Sciences (No. 2018253); National Natural Science Foundation of China (No. 51875545).

Conflict of interest

The authors declare no competing interests.

ORCID iD

Yu Lin https://orcid.org/0000-0002-9456-5138

References

[1] Palmer C and Loewen E G 2005 *Diffraction grating handbook* 6th (Rochester: Newport Corporation)
[2] Lalanne P, Astilean S, Chavel P, Cambril E and Launois H 1999 Design and fabrication of blazed binary diffractive elements with sampling periods smaller than the structural cutoff *J. Opt. Soc. Am.* A **16** 1143–56
[3] Lalanne P and Chavel P 2017 Metalenses at visible wavelengths: past, present, perspectives *Laser Photon. Rev.* **11** 1600295
[4] Zhu A Y, Chen W T, Sisler J, Yousef K M A, Lee E, Huang Y W, Qiu C W and Capasso F 2018 Compact aberration-corrected spectrometers in the visible using dispersion-tailored metasurfaces *Adv. Opt. Mater.* **7** 1801144
[5] Zhu A Y, Chen W-T, Khorasaninejad M, Oh J, Zaidi A, Mishra I, Devlin R C and Capasso F 2017 Ultra-compact visible chiral spectrometer with meta-lenses *APL Photonics* **2** 036103
[6] Yang Z, Albrow-Owen T, Cai W and Hasan T 2021 Miniaturization of optical spectrometers *Science* **371** eabe0722
[7] Wan W, Qiao W, Pu D, Li R, Wang C, Hu Y, Duan H, Guo L J and Chen L 2020 Holographic sampling display based on metagratings *iScience* **23** 100773
[8] Rajabalipanah H, Momeni A, Rahmanzadeh M, Abdolali A and Fleury R 2022 Parallel wave-based analog computing using metagratings *Nanophotonics* **11** 1561–71
[9] Deng Z L *et al* 2020 Full-visible transmissive metagratings with large angle/wavelength/polarization tolerance *Nanoscale* **12** 20604–9
[10] Phan T, Sell D, Wang E W, Doshay S, Edee K, Yang J and Fan J A 2019 High-efficiency, large-area, topology-optimized metasurfaces *Light. Sci. Appl.* **8** 48
[11] Raadi Y and Alu A 2022 Metagratings for efficient wavefront manipulation *IEEE Photon. J.* **14** 1–13
[12] Meng Y, Hu F, Liu Z, Xie P, Shen Y, Xiao Q, Fu X, Bae S H and Gong M 2019 Chip-integrated metasurface for versatile and multi-wavelength control of light couplings with independent phase and arbitrary polarization *Opt. Express* **27** 16425–39
[13] Meng Y, Hu F, Shen Y, Yang Y, Xiao Q, Fu X and Gong M 2018 Ultracompact graphene-assisted tunable waveguide couplers with high directivity and mode selectivity *Sci. Rep.* **8** 13362
[14] Giusfredi G 2019 *Physical Optics: Concepts, Optical Elements, and Techniques* (Cham: Springer)
[15] Oliva M, Michaelis D, Fuchs F, Tünnermann A and Zeitner U D 2013 Highly efficient broadband blazed grating in resonance domain *Appl. Phys. Lett.* **102** 203114
[16] Serebryannikov A E, Lalanne P, Petrov A Y and Ozbay E 2014 Wide-angle reflection-mode spatial filtering and splitting with photonic crystal gratings and single-layer rod gratings *Opt. Lett.* **39** 6193–6
[17] Yu N, Genevet P, Kats M A, Aieta F, Tetienne J P, Capasso F and Gaburro Z 2011 Light propagation with phase discontinuities: generalized laws of reflection and refraction *Science* **334** 333–7
[18] Sun S, He Q, Xiao S, Xu Q, Li X and Zhou L 2012 Gradient-index meta-surfaces as a bridge linking propagating waves and surface waves *Nat. Mater.* **11** 426–31
[19] Aalizadeh M, Serebryannikov A E, Ozbay E and Vandenbosch G A E 2020 A simple Mie-resonator based meta-array with diverse deflection scenarios enabling multifunctional operation at near-infrared *Nanophotonics* **9** 4589–600
[20] Kato Y, Omori K and Sanada A 2021 D-band perfect anomalous reflectors for 6G applications *IEEE Access* **9** 157512–21
[21] Memarian M, Li X, Morimoto Y and Itoh T 2017 Wide-band/angle blazed surfaces using multiple coupled blazing resonances *Sci. Rep.* **7** 42286
[22] Ra'di Y, Sounas D L and Alu A 2017 Metagratings: Beyond the limits of graded metasurfaces for wave front control *Phys. Rev. Lett.* **119** 067404
[23] Deng Z L, Li F J, Li H, Li X and Alù A 2022 Extreme diffraction control in metagratings leveraging bound states in the continuum and exceptional points *Laser Photon. Rev.* **16** 2100617
[24] Ra'di Y and Alù A 2018 Reconfigurable metagratings *Acs Photonics* **5** 1779–85
[25] Rabinovich O and Epstein A 2020 Dual-polarized all-metallic metagratings for perfect anomalous reflection *Phys. Rev. Appl.* **14** 064028
[26] Epstein A and Rabinovich O 2017 Unveiling the properties of metagratings via a detailed analytical model for synthesis and analysis *Phys. Rev. Appl.* **8** 054037
[27] Dong X, Cheng J, Fan F and Chang S 2019 Low-index second-order metagratings for large-angle anomalous reflection *Opt. Lett.* **44** 939–42
[28] Dong X, Cheng J, Fan F, Zhang Z, Liu Y, Wang X and Chang S 2020 Extremely large-angle beam deflection based on low-index sparse dielectric metagratings *J. Phys. D: Appl. Phys.* **53** 245101
[29] Shi W, Gu J, Zhang X, Xu Q, Han J, Yang Q, Cong L and Zhang W 2022 Terahertz bound states in the continuum with incident angle robustness induced by a dual period metagrating *Photon. Res.* **10** 810
[30] Zhang Z *et al* 2020 Coherent perfect diffraction in metagratings *Adv. Mater. Weinheim* **32** e2002341
[31] Shi T, Wang Y, Deng Z L, Ye X, Dai Z, Cao Y, Guan B O, Xiao S and Li X 2019 All-dielectric kissing-dimer

metagratings for asymmetric high diffraction *Adv. Opt. Mater.* **7** 1901389
[32] Panda S S and Hegde R S 2022 A learning based approach for designing extended unit cell metagratings *Nanophotonics* **11** 345–58
[33] Tsitsas N L and Valagiannopoulos C 2020 Anomalous refraction into free space with all-dielectric binary metagratings *Phys. Rev. Res.* **2** 033526
[34] Liu F, Wang M and Zhang X 2021 Directional colour routing assisted by switchable Fano resonance in bimetallic metagrating *Nanophotonics* **10** 2497–507
[35] Shirley J W 1951 An early experimental determination of Snell's law *Am. J. Phys.* **19** 507–8
[36] Hugonin J P and Lalanne P 2021 RETICOLO software for grating analysis *arXiv e-prints* (arXiv:2101.00901)
[37] Lalanne P and Morris G M 1996 Highly improved convergence of the coupled-wave method for TM polarization *J. Opt. Soc. Am.* A **13** 779–84
[38] Lalanne P and Jurek M P 1998 Computation of the near-field pattern with the coupled-wave method for transverse magnetic polarization *J. Mod. Opt.* **45** 1357–74
[39] Moharam M G, Gaylord T K, Grann E B and Pommet D A 1995 Formulation for stable and efficient implementation of the rigorous coupled-wave analysis of binary gratings *J. Opt. Soc. Am.* A **12** 1068–76
[40] Polyanskiy M 2008 *Refractive index database* (available at: https://refractiveindex.info/)
[41] Liu C, He J, Zhou J, Xu J, Bi K, Chen J, Qiao L and Bai Y 2021 Broadband, high-efficiency and wide-incident-angle anomalous reflection in groove metagratings *Ann. Phys., Lpz.* **533** 2100149
[42] COMSOLMultiphysics® 2022 V. 6.0. cn.comsol.com. COMSOL AB (Stockholm: COMSOL Multiphysics®)
[43] Chen Y, Shu Z, Zhang S, Zeng P, Liang H, Zheng M and Duan H 2021 Sub-10 nm fabrication: methods and applications *Int. J. Extrem. Manuf.* **3** 032002